Society of Petroleum Engineers

SPE-191802-MS

Hydraulic Fracture and Reservoir Characterization for Determining Optimal Well Spacing in the Marcellus Shale

Piyush Pankaj and Priyavrat Shukla, Schlumberger; Payam Kavousi and Timothy Carr, West Virginia University

This paper was prepared for presentation at the SPE Liquids-Rich Basins Conference-North America held in Midland, TX, USA, 05-06 September 2018.

Abstract

Naturally fractured reservoirs such as the Marcellus shale require an integrated reservoir modeling approach to determine well spacing and well-to-well interference. The Marcellus Shale Energy and Environment Laboratory (MSEEL) is a joint project between universities, companies, and government to develop and test new completion technologies and acquire a robust understanding of the Marcellus shale. The study presented in this paper aims to reveal an approach to determine reservoir depletion with time through coupled geological modeling and geomechanical evaluation followed by completion and well performance history matching for a multiwell pad in the Marcellus shale.

The geomechanical model was prepared with interpreted vertical log data. A discrete natural fracture (DFN) model was created and used to determine the complexity of hydraulic fracture geometry simulated through complex fracture models on a two well pad. The microseismic data obtained during the hydraulic fracture simulations served as a constraining parameter for the hydraulic fracture footprint in these wells. Sensitivity to the DFN is realized by parametric variations of DFN properties to achieve a calibrated fracture geometry. Reservoir simulation and history matching the well production data confirmed the subsurface production response to the hydraulic fractures. Well spacing sensitivity was done to reveal the optimum distance that the wells need to be spaced to maximize recovery and number of wells per section.

Hydraulic fracture geometry was found to be a result of the calibration parameters, such as horizontal stress anisotropy, fracturing fluid leakoff, and the DFN. The availability of microseismic data and production history matching through integrated numerical simulation are therefore critical elements to bring unique representation of the subsurface reaction to the injected fracturing fluid. This approach can therefore be consistently applied to evaluate well spacing and interference in time for the subsequent wells completed in the Marcellus. With the current completion design and pumping treatments, the optimal well spacing of 990 ft was determined between the wells in this study. However, wells to be completed in the future need to be modeled due to the heterogeneity in the reservoir properties to ensure that wells are not either underspaced to cause well production interference or overspaced to create upswept hydrocarbon reserves in the formation.

By adopting the key learnings and approach followed in this paper, operators can maximize subsurface understanding and will be able to place their wellbore in a nongeometric pattern based on reservoir heterogeneity to optimize well spacing and improve recovery.

Introduction

As operators aggressively expand their operations for completing oil and gas wells in unconventional resources, reservoirs have shown disappointing single-digit recovery across various basins in North America. With an aim to improve the fundamental understanding to improve reservoir recovery while diminishing the impact on the environment, the US Department of Energy partnered with the National Energy Technology Laboratory and leading industry operators and service companies to establish a multidisciplinary team at the Marcellus Shale Energy and Environment Laboratory (MSEEL). The work in this laboratory has been so far spread across geology and geoscience applications and evaluations. As part of the program, wells were drilled and completed in Morgantown, West Virginia (Fig. 1); these were four production wells, MIP-3H, MIP-4H, MIP-5H, MIP-6H; two pilot holes, MIP-3 and MIP-4; and a microseismic and sampled observation well, MIP-SW (Ghahfarokhi et al. 2018; Carr et al. 2017). The MIP-3H and MIP-5H wells were completed by Northeast Natural Energy, LLC (NNE) in December 2015 whereas the two previously drilled production wells MIP-4H and MIP-6H were drilled and completed in 2011.

Figure 1—MSEEL outside Morgantown, West Virginia, USA. The MSEEL site consists of four horizontal production wells, MIP-3H, MIP-4H, MIP-5H, MIP-6H; two pilot holes, MIP-3 and MIP-4; and a microseismic and sampled observation well, MIP-SW (Ghahfarokhi et al. 2018).

The Marcellus has been an attractive play for oil and gas operators since its first wells were completed in 2004. Rig activity was highest in 2011 (Fig. 2) as operators had ventured out in exploring the unconventional shale gas assets. Fig. 3 shows the past eight years of production from IHS data for the Marcellus shale. An EIA report (EIA 2016) declared Marcellus shale to be the largest natural gas producing play in the US. The wells are typically landed in the organic-rich basal section above the Onondaga limestone and below the Tully limestone. The depth of the formation is generally approximately 3,500 ft (1067 m) to 6,000 ft (1829 m) and approximately 220 ft thickness. The shale pay is naturally fractured and has nano-Darcy-range permeability.

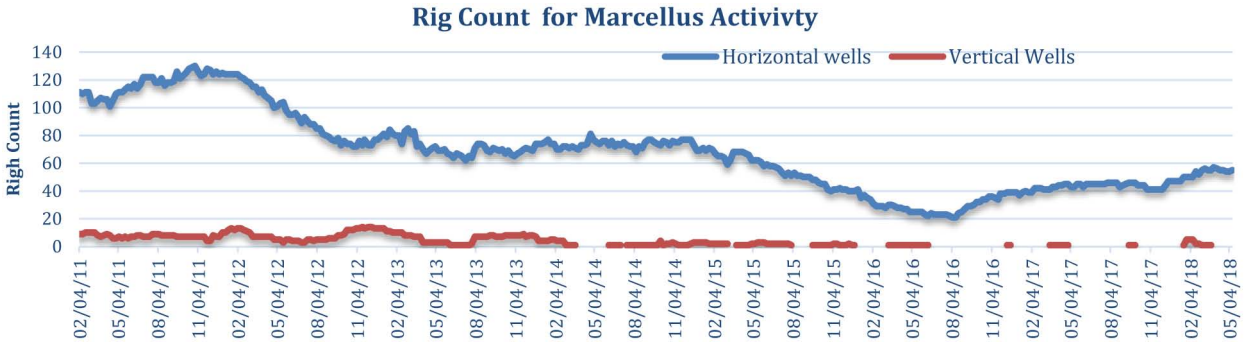

Figure 2—Marcellus shale rig count trends since 2011 (Source: Baker Hughes rig count).

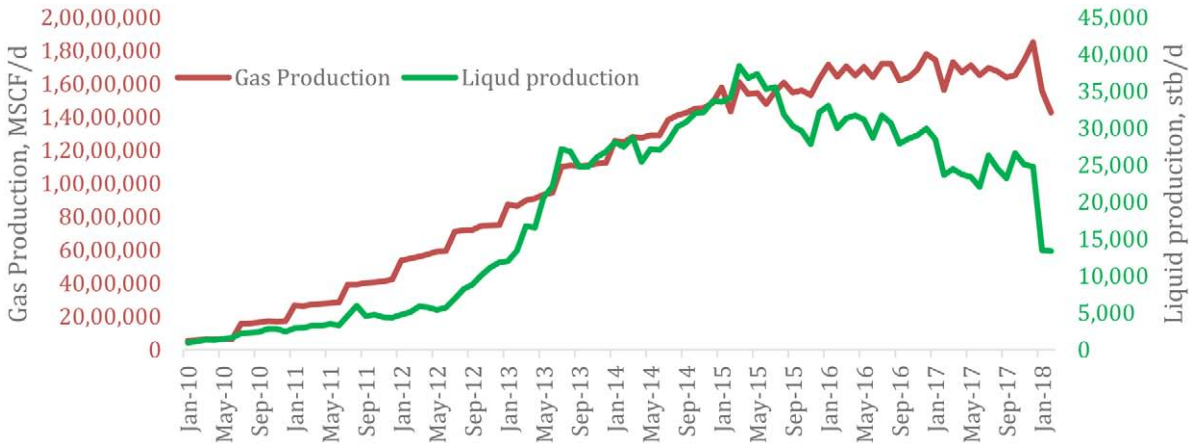

Figure 3—Marcellus production performance for the previous 8 years of activity (Source: IHS Markit).

Methodology

Evaluation of well performance was conducted through the integrated workflow shown in Fig. 4, which depicts the unconventional reservoir optimized completions workflow derived from the integrated "seismic-to-simulation" workflow (Cipolla et al. 2011a). These seamlessly integrate the various processes involved in well completion design/analysis and production optimization for unconventional reservoirs. The key steps include the construction of the geological model and detailed mechanical earth model (MEM) with the geomechanical and reservoir properties, completion description, calibration of the fracture model against treatment data and microseismic observation, simulation of fracturing treatment honoring the stress shadow, generation of the numerical grid model for reservoir description, and production simulation. Recent publications by Marongiu-Porcu et al. (2015), Pankaj et al. (2015), Weng (2011), Offenberger et al. (2013), Maxwell et al. (2011), Liu et al. (2013), Cipolla et al. (2011b), and Ejofodomi et al. (2011) presented and used this complete workflow or some of its components involving detailed reservoir characterization, completion design based on reservoir and completion quality, fracture simulation, calibration against microseismic data, and production matching and simulation. Minimum horizontal stress in the area is 6,500 psi, and stress anisotropy varies by 1.5% to 6%. Overburden stress is approximately 8,800 psi. Maximum horizontal stress is oriented along N57E, which follows the induced fracture trends from image log.

The complex model allows one to model the fracture geometry by predicting the interaction of hydraulic fractures with the pre-existing heterogeneity (planes of weakness or natural fractures) in the formation. The fracture model simulates fracture propagation, rock deformation, stress shadow, and fluid and proppant flow in the complex fracture network. The model solves the problem of fluid flow in the fracture network and the elastic deformation of the fractures, which has similar assumptions and governing equations to those of conventional pseudo-3D fracture models. However, instead of solving the problem for a single

planar fracture, the complex fracture model solves these equations for the complete description of complex fractures consisting of numerous fracture planes. The branching of the hydraulic fractures at the intersection with the natural fracture leads to the development of a nonplanar, complex fracture pattern (Weng 2014). The interaction of induced fractures with the natural fractures is governed by the work presented by Gu and Weng (2010), which was validated with carefully designed experiments conducted at a rock mechanics laboratory.

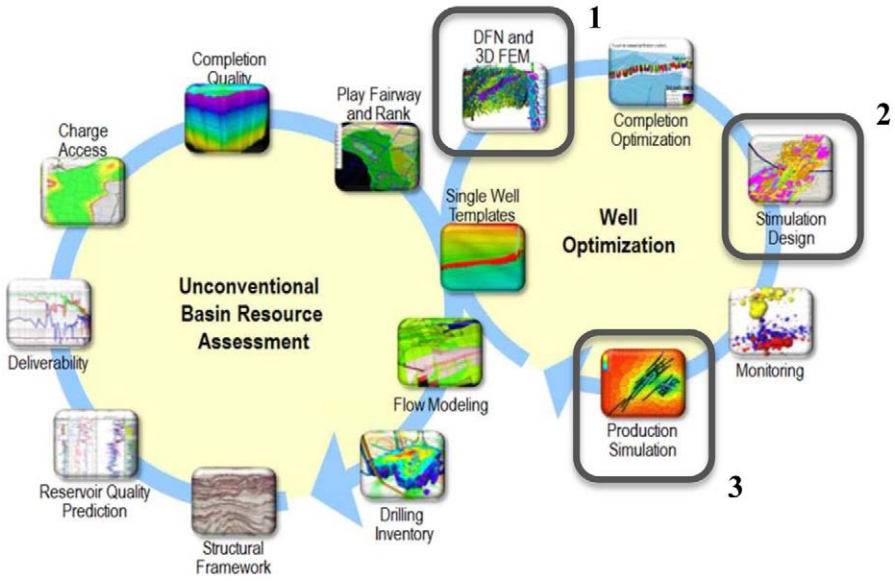

Figure 4—Single- or multiple-well pad completion optimization workflow.

Additionally, the evaluation of geomechanical property change due to the producing well conditions for future well planning needs to be evaluated. For this purpose, the workflow presented by Pankaj et al. (2016) (Fig. 5) can be used. The workflow derives the updated stresses from the depletion of the parent wellbore to model offset well/infill well fracture geometries. However, this falls outside the scope of this work, and we will limit the discussion to the workflow shown in Fig. 4 following steps 1, 2, and 3 highlighted. We have used a heat map approach instead to determine the optimum well spacing scenario.

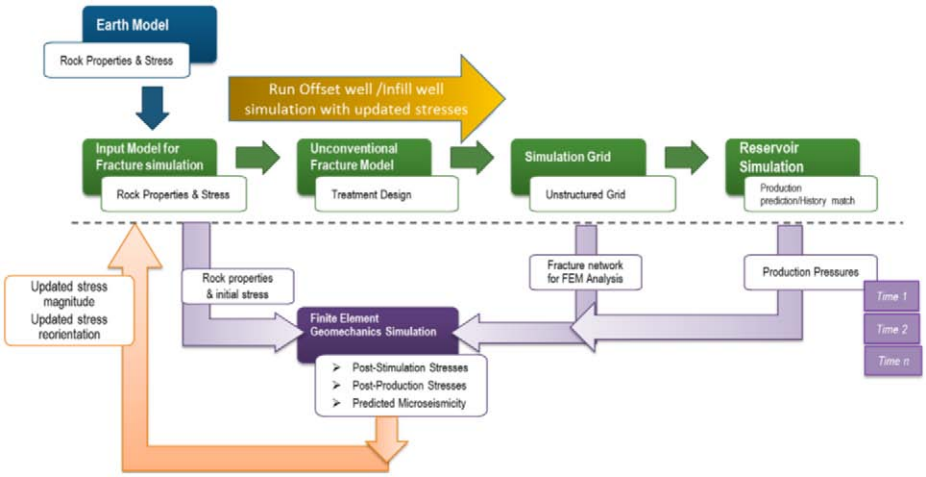

Figure 5—Fracture modeling for predicting the impact of fracture hits [modified from Pankaj et al. (2016)].

Wells MIP-3H and MIP-5H were analyzed using the aforementioned workflow (Fig. 4) through complex fracture models and numerical simulations for production history matching. The static geocellular model

for fracture modeling was created using well data from the pilot wellbores MIP-3 and MIP-4. A multilayer geocellular model that included the structural dip observed from geological surfaces was created with a vertical resolution of 5 ft. All petrophysical and geomechanical data were populated in the model using the pilot wellbore logs. Fig. 6 shows the cross section of minimum horizontal stress across MIP-3H and MIP-5H. Both wells are landed in the same zone with a high stress layer just below but lower stress layers above. Correspondingly, the hydraulic fractures are expected to grow upward, breaching the low-stress layers. However, there are higher-stress layers above, and fractures are expected to be contained in height at those layers.

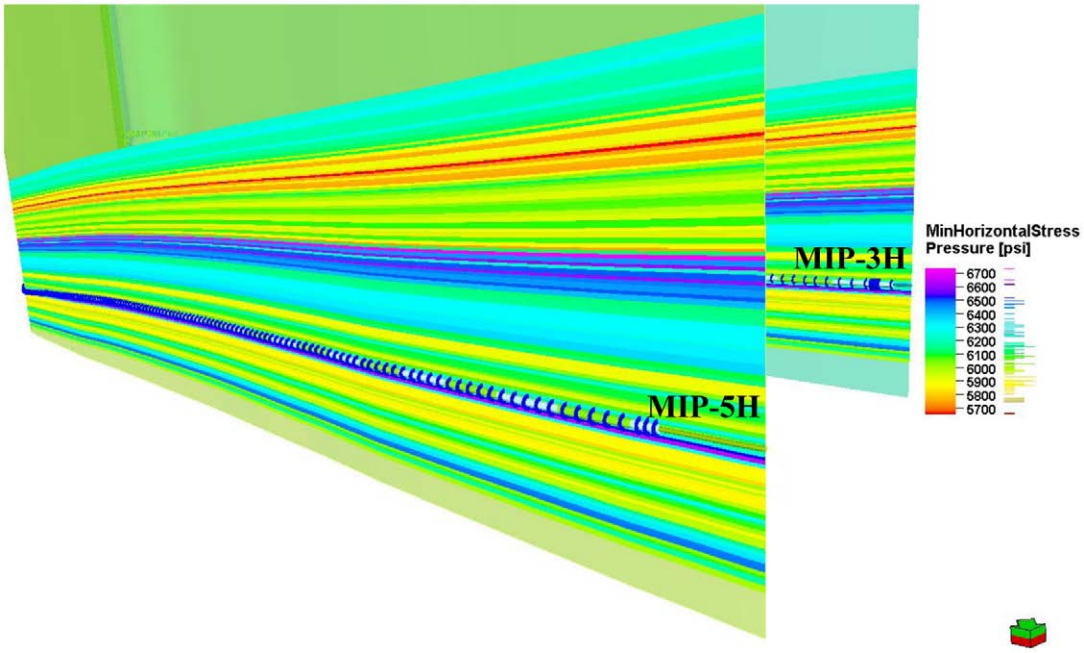

Figure 6—MIP-3H and MIP-5H vertical stress distribution showing well landing.

Because it is known that the Marcellus shale has natural fractures, the reservoir model was prepared with the description of natural fractures. Hydraulic fracture monitoring using microseismic data on these wells also demonstrates the presence of natural fractures owing to the wide and dispersed fracture footprint. Natural fractures in the model were created using the image log data to describe the distribution of natural fractures in the area. Two sets of natural fractures were identified. A N83E trend was identified on image logs, and N59W is the regional natural fracture description in the area (Wilson et al. 2016). Table 1 describes the two natural fracture sets. Vertical well image logs suggested open and healed natural fractures trending at N58E and N88E, respectively, and microseismic data also reveal that hydraulic fractures seem to follow the open natural fracture trend, and coincides with the maximum stress trend (Wilson et al. 2016). Figs. 7a and 7b show vertical well and microseismic fracture trends. The resulting natural fracture network cross section thus obtained is shown in Fig. 8a. The fracture modeling was performed using a complex fracture model (Wu et al. 2012) that can model the hydraulic fracture complexity and interaction in the presence of natural fractures. MIP-3H was completed with 28 stages, and MIP-5H was completed with 30 stages. Stages 15, 16, 17, 18, 19, 27, and 28 in MIP-3H had four perforation clusters per stage and rest of the stages had five clusters per stage. In MIP-5H, stage 1 had three clusters per stage, and the rest of the stages had five clusters per stage. To model the hydraulic fractures, pump schedules were created from the treatment data pumped during the fracturing job. A typical design schedule for these wells is shown in Table 2. A total of 253,523 barrels (bbl) (9,054 bbl per stage) was pumped in MIP-3H and 237,175 bbl (7,906 bbl per stage) in MIP-5H, and the proppant totals were 11,257,640 pounds (lbm) and 11,088,100 lbm, respectively. Hence,

the normalized proppant amount for MIP-3H and MIP-5H was 1,858 lbm/ft and 1,917 lbm/ft, respectively. Fig. 8b shows the resulting hydraulic fracture geometries obtained for the two wells. As noted previously from the stress distribution, the fractures have more upward height growth than towards the bottom because of the preferred pathway provided due to the horizontal stress distribution in the layers vertically.

Table 1—Natural fracture distribution statistics for the model.

Property	Length (ft)	Orientation (degree)	Spacing (ft)
Fracture set 1	500	83	20
Fracture set 2	300	59	20

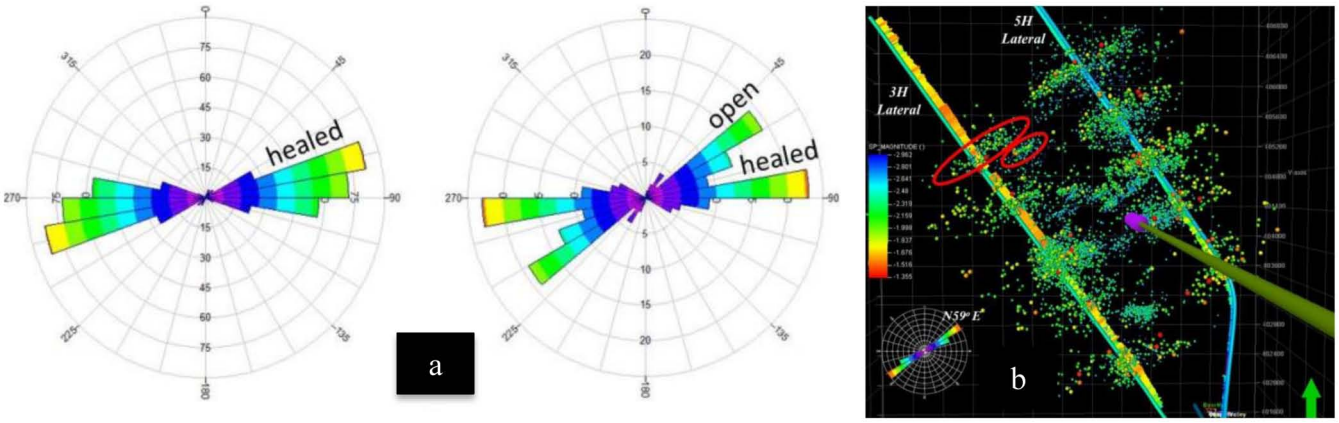

Figure 7—(a) Open and healed natural fracture systems picked from vertical well image log showing N58E and N88E fracture trends. (b) Microseismic data showing fracture azimuth along N59E that also matches maximum horizontal stress direction (Wilson et al. 2016).

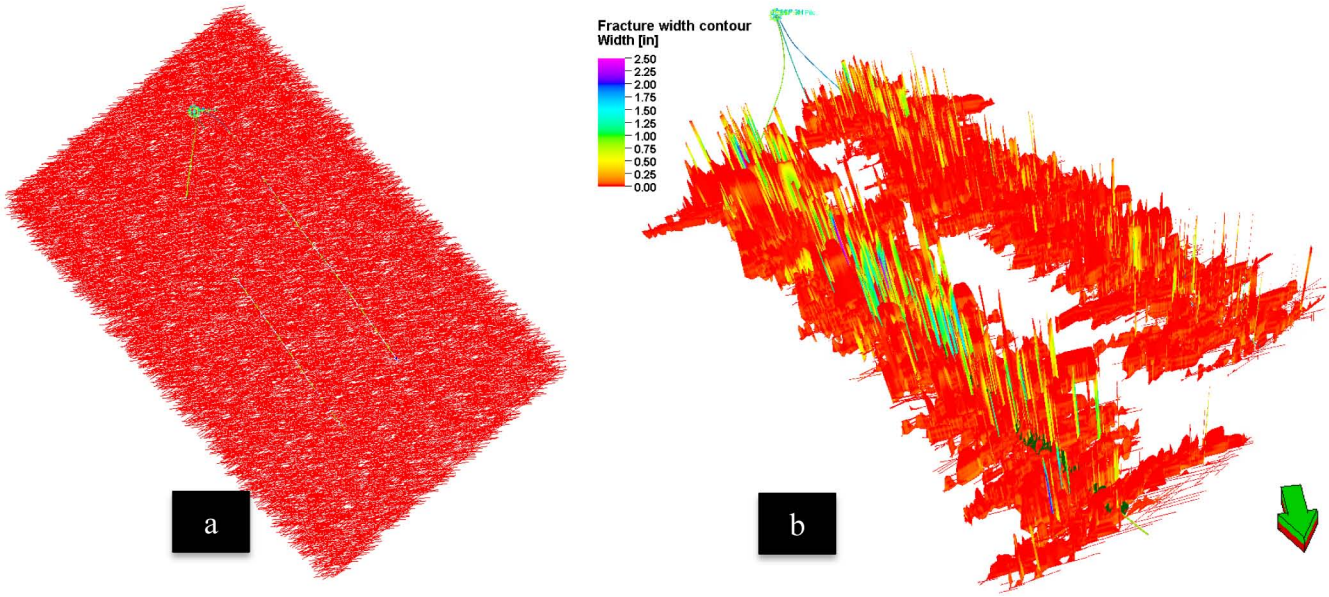

Figure 8—(a) Statistical natural fracture network distribution in the model. (b) Hydraulic fracture geometries for MIP-3H and MIP-5H.

Two techniques were adopted to calibrate the hydraulic fracture geometries. First, the treatment pressure data recorded from the field operation were used to match the pressure from the fracture simulation in the model. This gave a calibration of geomechanical model and minimum in-situ stress distribution, leakoff, and the frictional pressure drop in the flow-string. Second, the microseismic data available for both wells

were used to match the fracture azimuth and footprint. At the end, both calibration pieces were honored, and a reasonable match for fracture geometries was obtained (Fig. 9).

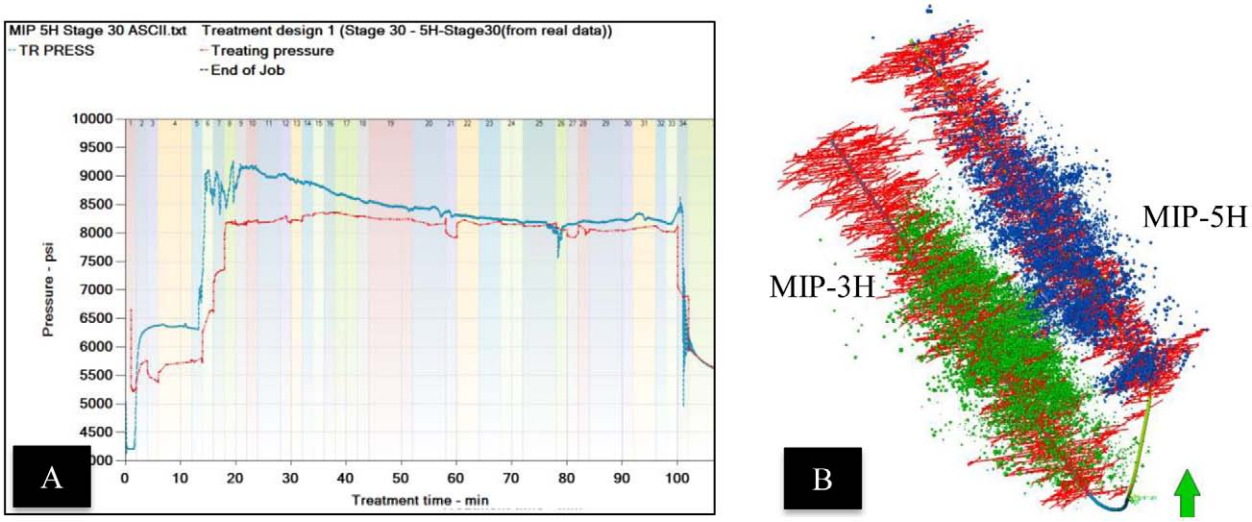

Figure 9—(a) Treating pressure match for stage 30 on MIP-5H. (b) Hydraulic fractures along with microseismic events on MIP-3H and MIP-5H showing good match.

Treating pressure match was performed on three stages of both wells as part of the calibration. The three stages were selected in the heel, middle, and toe part of the well to capture the heterogeneity across the lateral. The resulting calibration factors were applied to the neighboring stages. For MIP-3H, stages 1, 14, and 28 were pressure matched, and for MIP-5H, stages 1, 15, and 30 were pressure matched. For achieving the match, slight modifications were made in the stress magnitude (approximately 200 psi), leak-off, and frictional pressure drop. The end of job net pressure was matched as recorded from the field data.

Upon fracture calibration, the productive fracture volume in the model was estimated by the production history matching of the real production data. An unstructured production grid with almost 1 million grid cells was created to capture the complex fracture geometry and heterogeneity. The minimum fracture cell size in the model was set as 10 ft, and maximum cell size was 100 ft. Fig. 10 shows the pressure variation in the production grid across the topmost layer upon production simulation using a numerical simulator. The simulation was initialized in equilibration because these were the first wells drilled in the area and the wells were in static in-situ state.

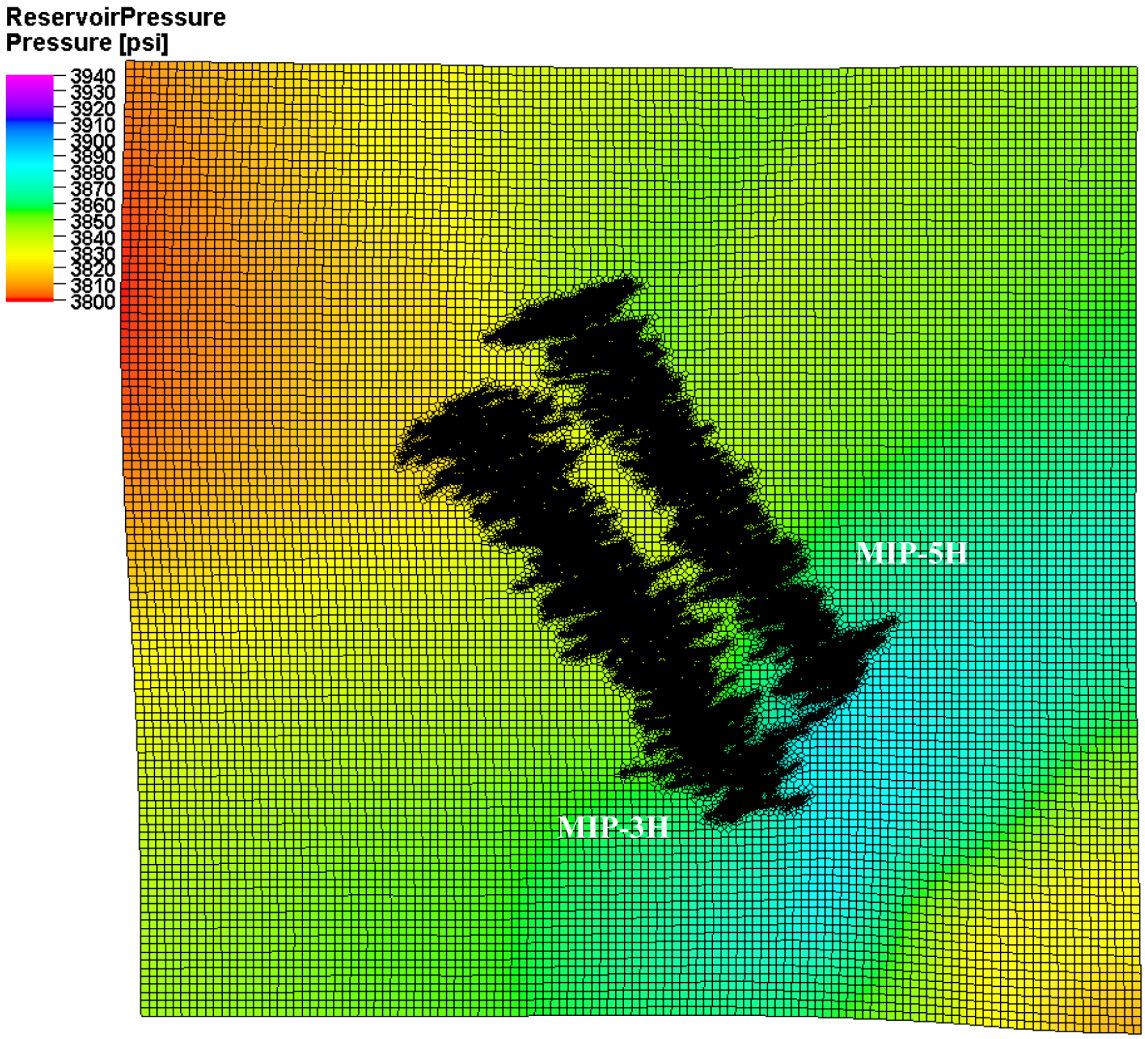

Figure 10—Production grid containing hydraulic fracture properties from MIP-3H and MIP-5H. The grid has approximately 1 million cells. The property shown is reservoir pressure.

Fig. 11 and Fig. 12 show the production history matching results for the two wells. The history match was run under the rate control mode, and bottomhole pressure response was matched. The initial part 1-year period shows a good match, but the increased production rate after that saw the history match deteriorating.

A sudden increase of well gas production in late 2016 appears to be why the history matching of the bottomhole pressure is hard to attain. We suggest that this abrupt gas production increase might have caused a strong drag force around the proppants in the hydraulic fractures. The high gas rate in the fractures is likely to transport some proppant and cause partial fracture closing and, as a result, a lower productivity. To reflect this in the history matching process, we lowered the productivity index of the well and attained a history match.

In addition, the MIP-3H well was washed with water and nitrogen to be cleaned for a production logging operation in February 2017. The washing operation could have damaged the well by a blockage of gas production. Therefore, lowering the productivity was assumed to be a controlling factor for obtaining a history match.

Fig. 11 and Fig.12 show the bottomhole pressure and water production rate match for MIP-3H and MIP-5H under gas rate control mode. Both plots show a good match for the entire duration of the production history, which enables a reliable production forecast.

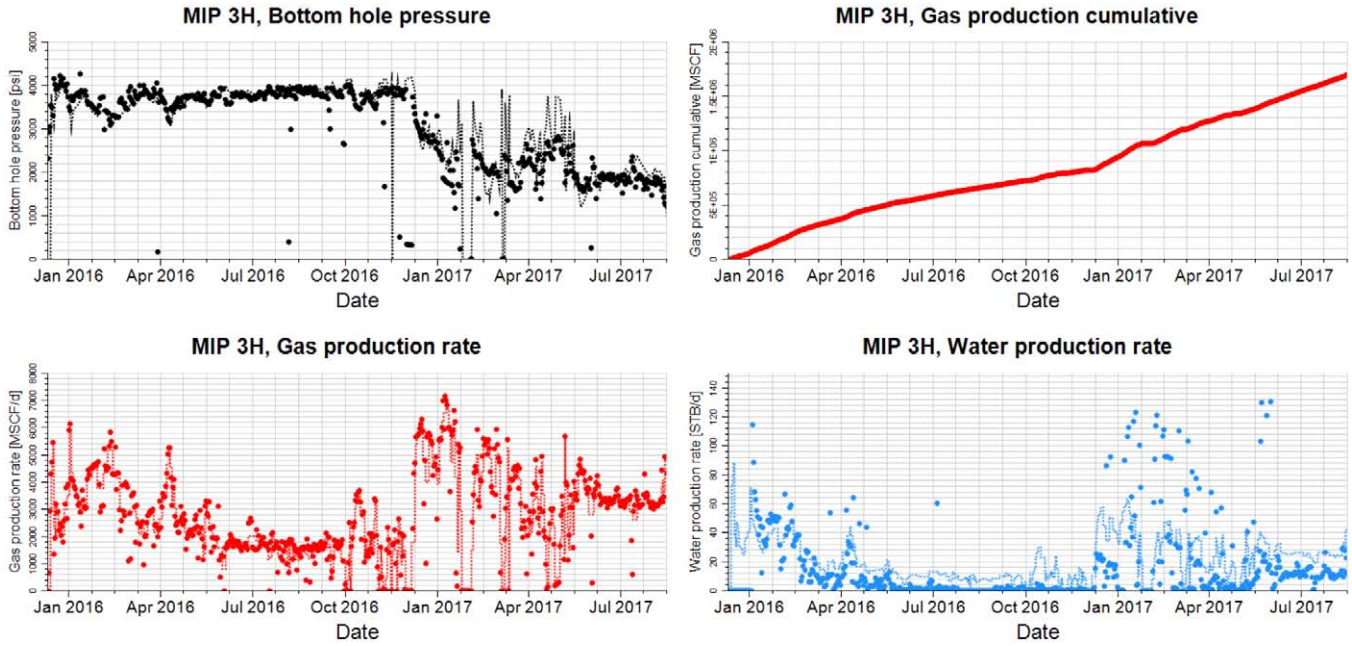

Figure 11—Production history match for MIP-3H showing bottomhole pressure and water production rate match under gas rate control mode.

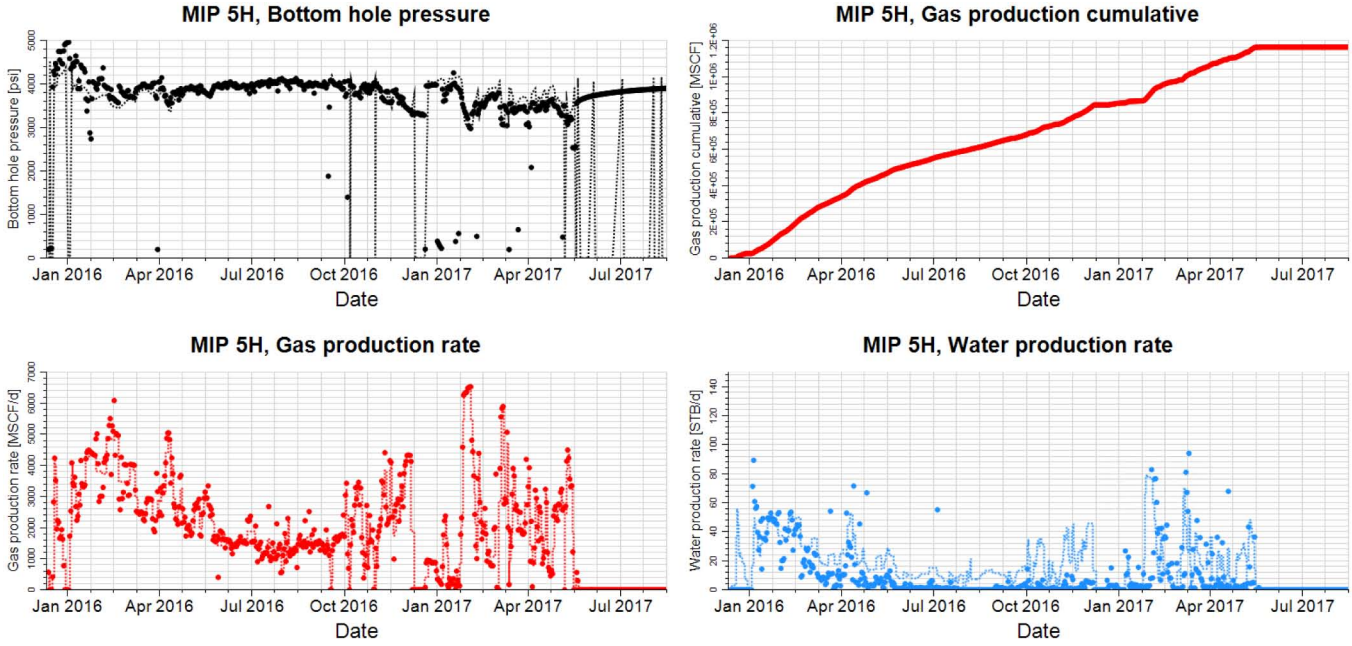

Figure 12—Production history match for MIP-5H showing bottomhole pressure and water production rate match under gas rate control mode.

Well Spacing

A hydraulic fracture is created to extend the contact surface area of the wellbore to the low-permeability reservoir through the means of pumping fluid and fracturing proppants. As the fractures are induced by pumping the fluid, the reservoir drainage for the wellbore can be extended through the additional contact created by the hydraulic fracture geometries. The well spacing decision is tightly integrated with the completion design and stimulation treatment pumped in the well. If the treatments pumped in the wells are tailored to cover the space and acreage between the wells, then the spacing is deemed optimal. However, if the reservoir is left unstimulated and undrained, the spacing and completion program can result in leaving

reserves behind because the hydraulic fracture did not simulate and produce the in-place rock effectively as shown in an example in the Fig. 13. The only means to access the rock between fractures is to drill an infill well.

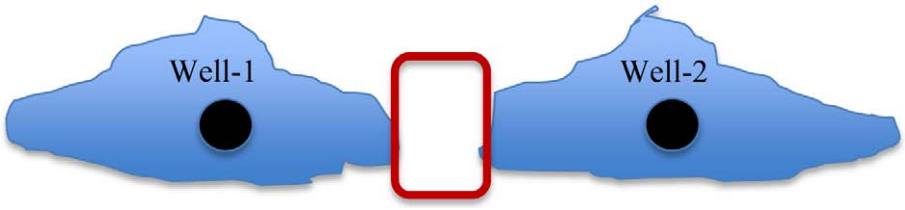

Figure 13—Example of sub-optimal well spacing as the fracture geometry from individual wells fails to cover the entire space between the wells shown in the red box.

Currently, the wells are spaced at 1730 ft, and the completion design for the well matches the microseismic data and production performance. Further, the executed treatment designs for MIP-3H and MIP-5H were evaluated by means of completion heat-map technique in which the fracture geometry along the wellbore is collapsed into a plane to visually identify the density and intensity of stimulation around wellbore. The heat maps for the hydraulic fracture count and propped fracture count along the wellbore are shown in Fig. 14 and Fig. 15, respectively, as a representation in a "gun-barrel" view. As the color changes from purple to red, the number count gradually decreases. It is observed that the wells MIP-3H and MIP-5H are in very limited hydraulic and propped fracture communication because the intensity of color for overlap is very minor at the intersection.

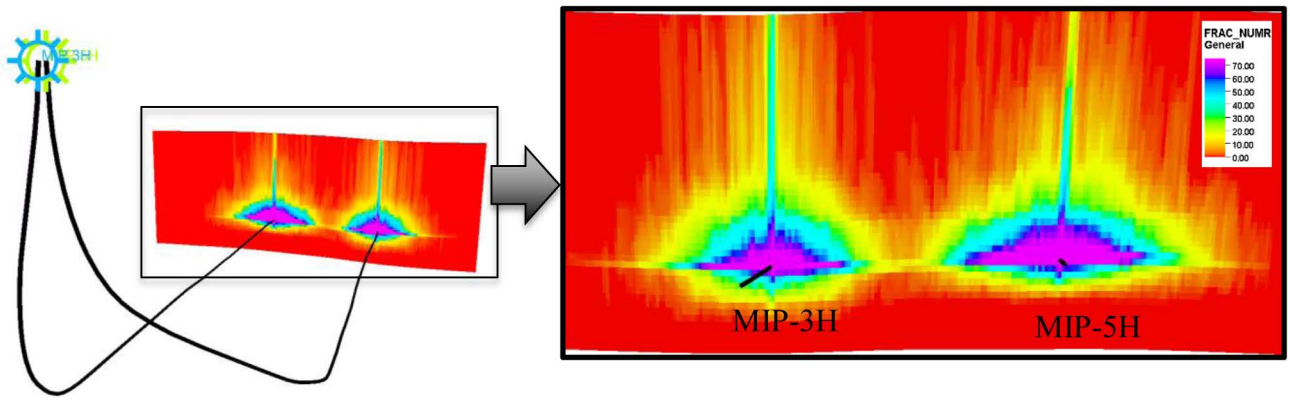

Figure 14—Hydraulic fracture heat map for MIP-3H and MIP-5H shows poor hydraulic coverage between the wells at the current spacing of 1735 ft.

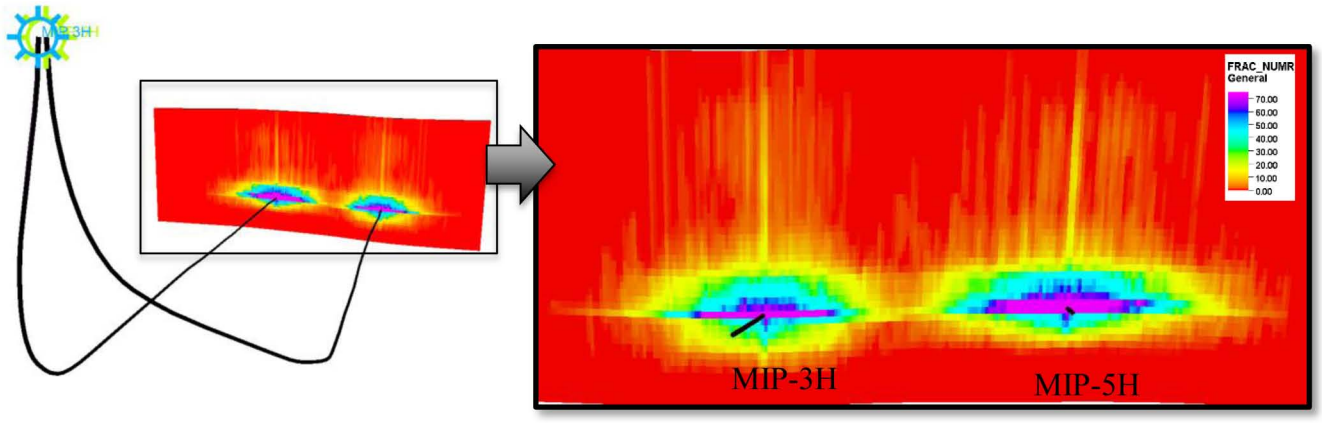

Figure 15—Propped fracture heat map for MIP-3H and MIP-5H shows poor hydraulic coverage between the wells at current spacing of 1735 ft.

As these treatments are pumped, the calibrated model, as explained in the previous sections, with the history matching along with heat map results shows that the well has not effectively drained the region between the wells MIP-3H and MIP-5H.

Additional sensitivity for well spacing at 990 ft was run, and it is observed that the fractures have greater overlap and the wells' performance is not degraded as compared to the current 1735 ft. Reducing the well spacing further, below 990 ft, with the current pump schedule and completion designs, the wells would have hydraulic fractures overlapping to a greater degree and therefore competing for the same reservoir rock. Optimal well spacing is therefore determined at 990 ft. With varying the proppant loading for the treatment, it is observed with sensitivity analysis that the fracture half-length increases with proppant loading (Fig. 16). At the current design of approximately 1900 lbm/ft, just slightly over 450 ft half-length is achieved. Propped fracture length is close to 350 ft away from the wellbore. Therefore, the ideal well spacing is approximately 990 ft at 1900 lbm/ft treatment design, which will not leave substantial volume of rock between wells undrained.

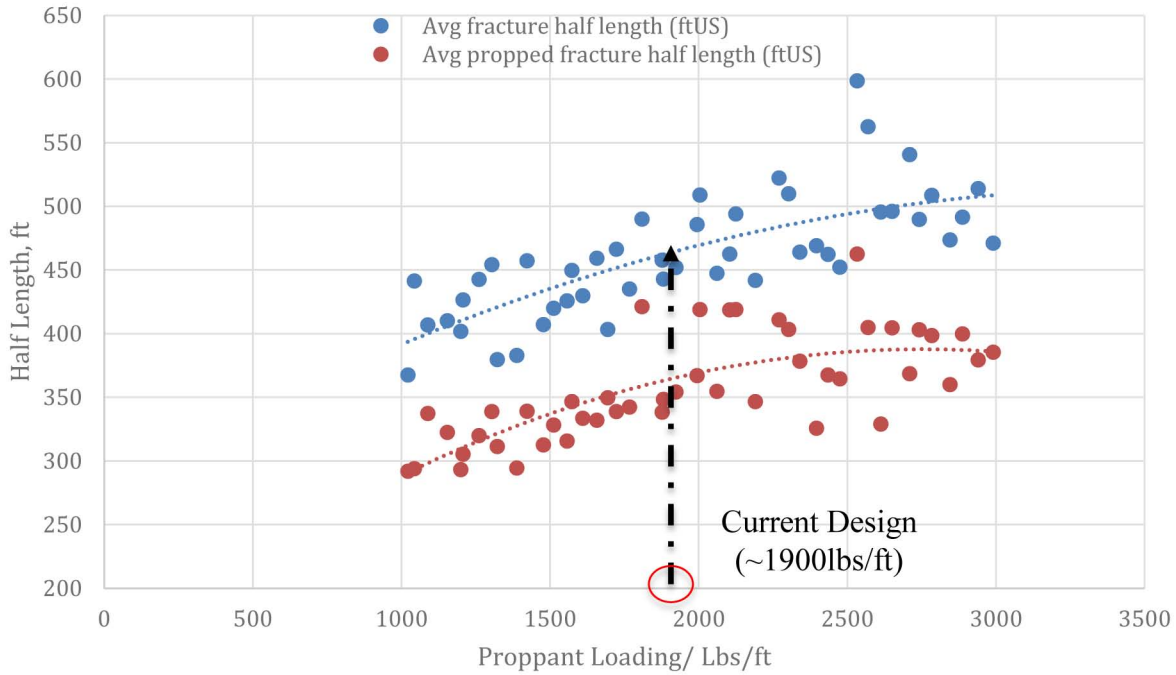

Figure 16—Sensitivity analysis for fracture geometry at different proppant loading.

We also compared the total fracture surface area with different well spacing scenarios (Fig. 17). As the wells get closer, the fracture surfaces from the two wells complete and overlap, whereas when the well spacing is increased, the fractures from the individual wells are farther apart, and hence lesser interference is expected. Optimal well spacing could be a point of inflection of the curve as the slope changes, shown as the intersection of the red lines for slope to the trend line. The intersection of the trend line slope indicates that the well spacing is transitioning from an extreme overlapping and interference regime between the wells towards a classic single-well behavior with minimal overlap of the fractures from the two wells. We would like to coin this method to determine the well spacing as the "well-spacing typing plot". Since the fractures from the wells may not be equal due to heterogeneity and effective lengths are normally shorter than the hydraulic lengths, some degree of fracture overlap is desired. The plot shows that the wells may have an optimal spacing of approximately 1000 ft. We have additionally tested the completion heat map approach to determine the overlapping of fracture geometries from the two wells.

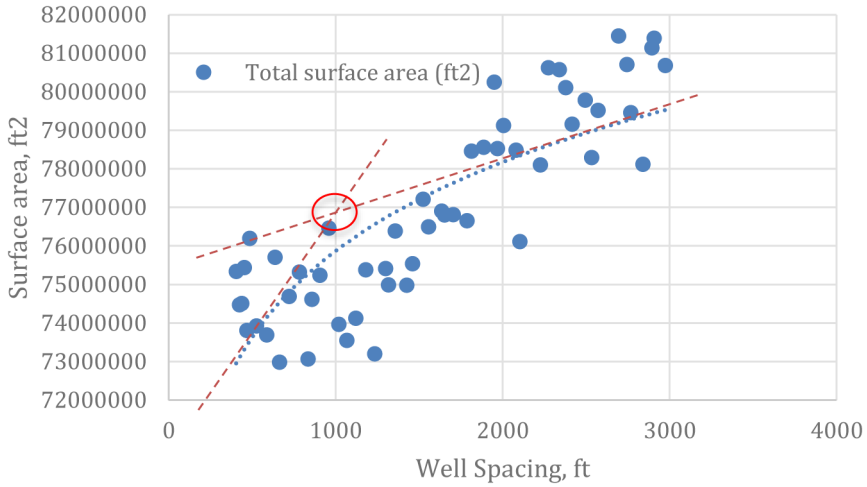

Figure 17—Sensitivity analysis for fracture surface area with well spacing, "Well-Spacing Typing Plot".

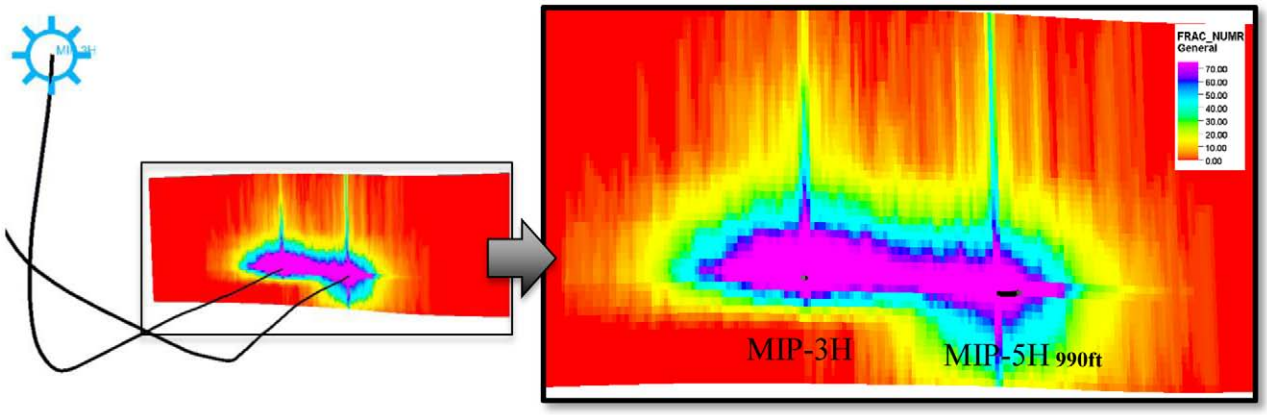

Figure 18—Hydraulic fracture heat map for MIP-3H and MIP-5H at 990ft spacing show improved hydraulic coverage in between the wells.

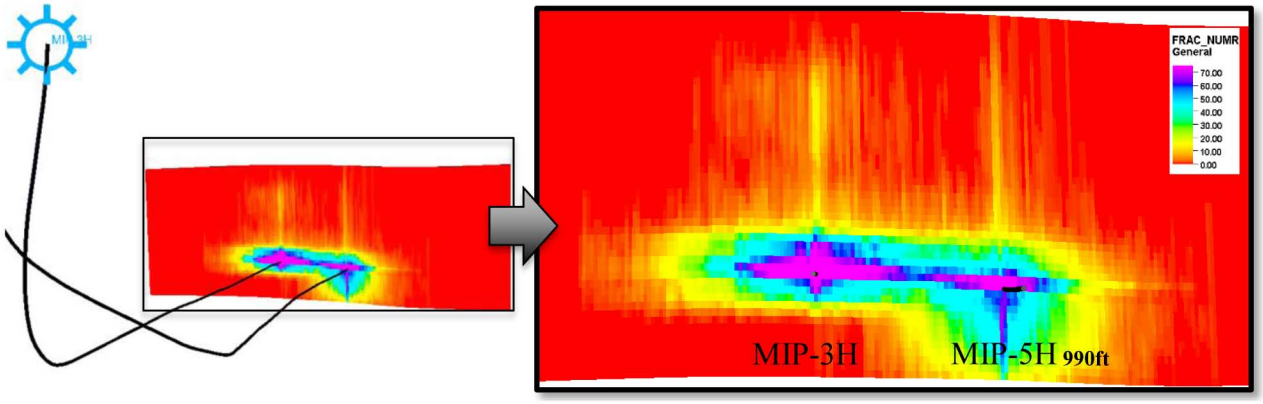

Figure 19—Propped fracture heat map for MIP-3H and MIP-5H at 990ft spacing show improved hydraulic coverage in between the wells.

It is also noticed in the heat maps, that the fracture geometry of the MIP-5H at 990ft well spacing tends to have some additional height growth in the lower side of the wellbore. This is caused by the geomechanical property variation. To supplement the heat map, a plan view of the fractures in Fig. 20 shows that some propped fractures along the wellbore overlap marginally when the wells are spaced at 990ft spacing whereas at the current spacing of the wells, the fractures are far apart and not interfering with each other. The fracture geometry is also affected when the wells are brought closer due to the stronger stress shadow impact. The footprint of hydraulic fracture in the well MIP-3H moves slightly more towards the east direction as the stress shadow from MIP-5H impacts the geometry.

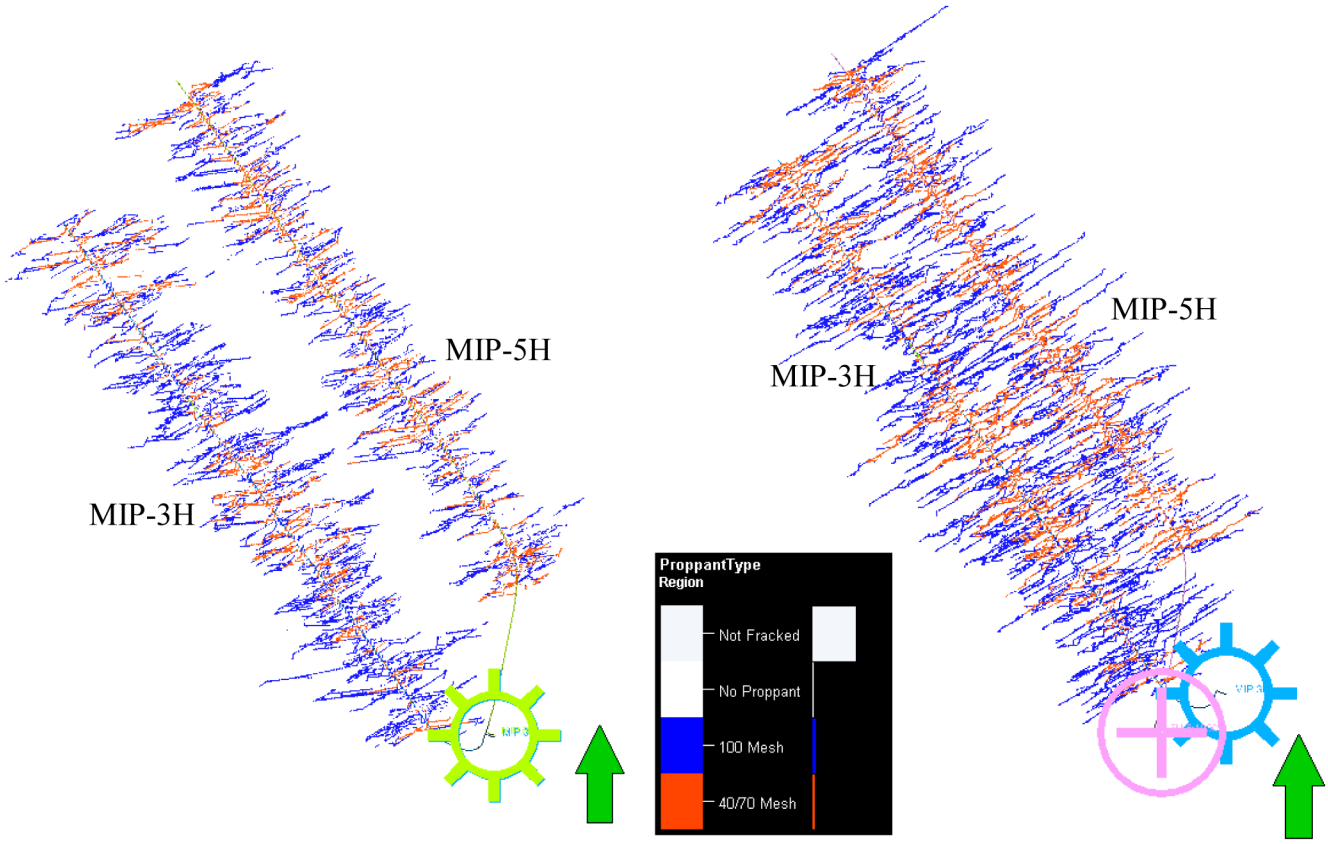

Figure 20—Plan view of the hydraulic fracture footprint and proppant distribution at a) current well spacing and b) 990ft well spacing. Greater overlap is observed in the case when wells are closely spaced and additionally impacts the fracture geometry by stronger stress shadow influence.

When production simulation was run to compare the two cases of current well spacing and 990ft well spacing, it is seen that with the stress shadow allowing fracture in MIP-3H moves to the left, away from the MIP-5H, the well may have a better potential as the bottom hole pressure with the same rate control applied to both cases show improvement of 17% when the wells are closer (Fig. 21). Therefore, close spacing may improve the well productivity due to stronger stress shadow. Actual improvement quantification may however need some pilot tests at closer well spacing in the future development around the area.

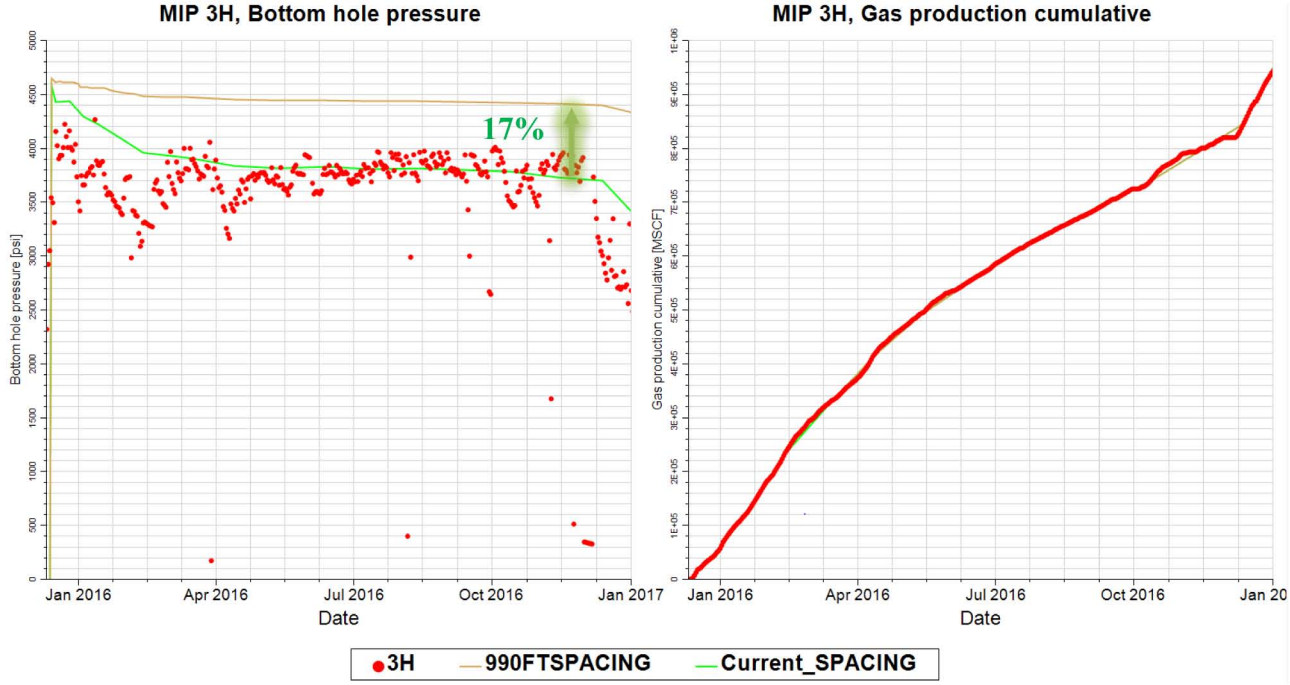

Figure 21—Improved well performance is feasible when the wells are closely spaced due to the impact of well-to-well stress shadow

Conclusions

MIP-3H and MIP-5H wells were used to perform a fracture calibration and production history match workflow to demonstrate the methodology followed for unconventional pad development. Well spacing is tightly integrated to the type of fracture treatments pumped on the wellbores. Small sized fracture treatment may allow wells to be placed closer as the fractures are smaller in footprint. The key lessons learnt during this workflow are captured below:

1. Multi-well pad development needs to capture inter-well communication for stress shadow, fracture interference and production interference using multipoint calibration process. The calibration of the model is attained through treatment pressure matching incorporating the microseismic measurement data as well as production history matching.
2. Natural fractures play a big role in the final fracture geometry and complexity in the Marcellus shale. Multiple realizations of natural fractures were tested using complex fracture models. Image logs, core analysis and seismic data provide valuable information on the natural fracture distribution in the reservoir and reduce the uncertainty in natural fracture distribution.
3. All wells should be gridded in a multi-well grid to capture the production interference between the wells. When wells are fractured at different times, and come on production at different times, then it is recommended to incorporate finite element geomechanical simulations to capture changes in stress magnitude and direction

4. Production history matching makes a model reliable to readily forecast forecast future production performance.
5. Sensitivity analysis for well spacing and well completion allows determining the optimal spacing at a given well stimulation design. "Well-Spacing Typing Pot" has been introduced to determine the optimal well spacing through multiple sensitivity analysis on a calibrated model. This could be applied in any other play for optimizing well spacing.
6. Completion heat maps allow much improved visual analysis for well spacing. Some degree of hydraulic and propped fracture overlap in the heat map is required to ensure the reservoir rock in between the wells is not left undrained. No overlap of the heat maps from wells would propose poor drainage efficiency and extreme overlap of the well's heat map would indicate that the wells may compete for the same reservoir rock.

Acknowledgments

The authors would like to thank Schlumberger, Marcellus Shale Energy and Environment Laboratory (MSEEL), West Virginia University, US Department of Energy, National Energy Technology Laboratory (MSEEL supported by DOE Award no.: DE-FE0024297, and all the MSEEL consortium members for their support and permission to publish this study.

References

1. Carr, T. R., Wilson, T., Kavousi, P. 2017. Insights from the Marcellus Shale Energy and Environment Laboratory (MSEEL). Presented at the Unconventional Resources Technology Conference, Austin, Texas, USA, 24-26 July. URTEC-2670437-MS. https://doi.org/10.15530/URTEC-2017-2670437
2. Cipolla, C. L., Fitzpatrick, T., Williams, M. J., et al. 2011a. Seismic-to-Simulation for Unconventional Reservoir Development. Presented at the SPE Reservoir Characterisation and Simulation Conference and Exhibition, Abu Dhabi, UAE, 9-11 October. SPE-146876-MS. https://doi.org/10.2118/146876-MS
3. Cipolla, C. L., Weng, X., Mack, M. G. et al. 2011b. Integrating Microseismic Mapping and Complex Fracture Modeling to Characterize Hydraulic Fracture Complexity. Presented at the SPE Hydraulic Fracturing Technology Conference, The Woodlands, Texas, USA, 24-26 January. SPE-140185-MS. https://doi.org/10.2118/140185-MS
4. EIA. 2016. Marcellus, Utica Provide 85% of U.S. Shale Gas Production Growth since Start of 2012. https://www.eia.gov/todayinenergy/detail.php?id=22252 (accessed 12 June 2018).
5. Ejofodomi, E., Baihly, J. D., Malpani, R. et al. 2011. Integrating All Available Data to Improve Production in the Marcellus Shale. Presented at the North American Unconventional Gas Conference and Exhibition, The Woodlands, Texas, USA, 14-16 June. https://doi.org/10.2118/144321-MS
6. Ghahfarokhi, P. K., Carr, T., Song, L. et al. 2018. Seismic Attributes Application for the Distributed Acoustic Sensing Data for the Marcellus Shale: New Insights to Cross-Stage Flow Communication. Presented at the SPE Hydraulic Fracturing Technology Conference and Exhibition, The Woodlands, Texas, USA, 23–25 January. https://doi.org/10.2118/189888-MS
7. Gu, H., and Weng, X. 2010. Criterion for Fractures Crossing Frictional Interfaces at Non-orthogonal Angles. Presented at the U.S. Rock Mechanics Symposium and 5th U.S.-Canada Rock Mechanics Symposium, Salt Lake City, Utah, 27–30 June. ARMA-10-198.
8. Ghahfarokhi, P. K., Carr, T., Song, L., Shukla, P., & Pankaj, P. (2018, January 23). Seismic Attributes Application for the Distributed Acoustic Sensing Data for the Marcellus Shale:

New Insights to Cross-Stage Flow Communication. Society of Petroleum Engineers. doi: 10.2118/189888-MS

9. Liu, H., Luo, Y., Li, X. et al. 2012. Advanced Completion and Fracturing Techniques in Tight Oil Reservoirs in Ordos Basin: A Workflow to Maximum Well Potential. Presented at the SPE Annual Technical Conference and Exhibition, San Antonio, Texas, 8–10 October. SPE-158268-MS. https://doi.org/10.2118/158268-MS
10. Marongiu-Porcu, M., Lee, D., Shan, D., & Morales, A. (2015, September 28). Advanced Modeling of Interwell Fracturing Interference: an Eagle Ford Shale Oil Study. Society of Petroleum Engineers. doi: 10.2118/174902-MS.
11. Maxwell, S. 2011. What Does Microseismic Tell us About Hydraulic Fracture Deformation: *CSEG Recorder* **36**: 31–45.
12. Offenberger, R., Ball, N., Kanneganti, K. et al. 2013. Integration of Natural and Hydraulic Fracture Network Modeling with Reservoir Simulation for an Eagle Ford Well. Presented at the Unconventional Resources Technology Conference, Denver, Colorado, USA, 12-14 August. URTEC-1563066-MS.
13. Pankaj, P., Geetan, S., MacDonald, R. (2015). Reservoir Modeling for Pad Optimization in the Context of Hydraulic Fracturing. Presented at the SPE Asia Pacific Unconventional Resources Conference and Exhibition, Brisbane, Australia, 9–11 November. https://doi.org/10.2118/176865-MS
14. Pankaj, P., Gakhar, K., and Lindsay, G. 2016. When to Refrac? Combination of Reservoir Geomechanics with Fracture Modeling and Reservoir Simulation Holds the Answer. Presented at the SPE Asia Pacific Oil & Gas Conference and Exhibition, Perth, Australia, 25-27 October. https://doi.org/10.2118/182161-MS
15. Weng, X. 2014. Modeling of Complex Hydraulic Fractures in Naturally Fractured Formation. *Journal of Unconventional Oil and Gas Resources*, **9**:114-135. https://doi.org/10.1016/j.juogr.2014.07.001
16. Weng, X., Kresse, O., Cohen, C.-E. et al. 2011. Modeling of Hydraulic-Fracture-Network Propagation in a Naturally Fractured Formation. *SPE Prod & Oper* **26** (4): 368–380. https://doi.org/10.2118/140253-PA
17. Wilson, T., Carr, T., Carney, B. J. et al. 2016. Microseismic and Model Stimulation of Natural Fracture Networks in the Marcellus Shale, West Virginia. *SEG Technical Program Expanded Abstracts 2016*: 3088-3092. https://doi.org/10.1190/segam2016-13866107.1
18. Wu, R., Kresse, O., Weng, X. et al. 2012, Modeling of Interaction of Hydraulic Fractures in Complex Fracture Networks. Presented at the SPE Hydraulic Fracturing Technology Conference, The Woodlands, Texas, USA, 6–8 February. SPE-152052-MS. https://doi.org/10.2118/152052-MS.